

A Novel Admittometric Sensor for Determination of Theophylline using FFT Coulometric Admittance Voltammetry and Flow Injection Analysis

Parviz Norouzi^{1,2,*}, Shirin Shahabi¹, Mustafa Aghazadeh³, Bagher Larijani^{4,*}, Nazanin Ghaheer¹

¹ Center of Excellence in Electrochemistry, School of Chemistry, College of Science, University of Tehran, Tehran, Iran

² Biosensor Research Center, Endocrinology & Metabolism Molecular-Cellular Sciences Institute, Tehran University of Medical Sciences, Tehran, Iran

³ Materials and Nuclear Research School, Nuclear Science and Technology Research Institute (NSTRI), P.O. Box 14395-834, Tehran, Iran

⁴ Endocrinology & Metabolism Research Center, Endocrinology & Metabolism Molecular-Cellular Sciences Institute, Tehran University of Medical Sciences, Tehran, Iran

*E-mail: norouzi@khayam.ut.ac.ir

Received: 31 May 2017 / Accepted: 23 September 2017 / Published: 12 October 2017

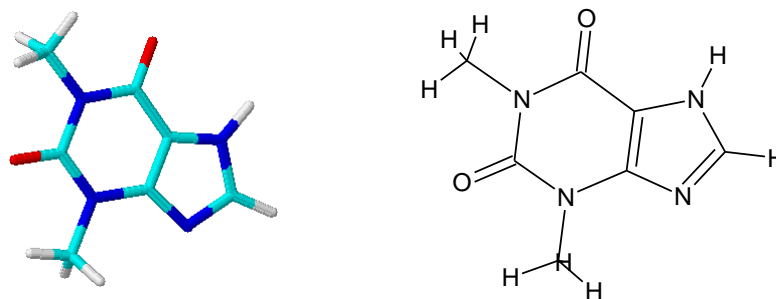
A new electrochemical analysis was established for the determination of Theophylline using FFT Coulometric Admittance Voltammetry (FFTC AV) technique and a new nanocomposite electrode, which was placed in a flow-injection system. The electrode was constructed by deposition of gold nanoparticles on mixture of multiwall carbon nanotube and chitosan casted on a carbon paste electrode containing SiC NPs and ionic liquid. The analyte response was calculated to obtain the charge changes, which was integration of the admittance in selected potential range, where the background admittance was subtracted. The electrode surface characterization was studied by electrochemical impedance spectroscopy and scanning electron microscopy techniques. As result, application of the new nanocomposite catalyzed electron transfer and causes a significant enhancement in the analyte response. It was found that the response enhanced proportionally with concentrations of Theophylline in a range from 2 to 100 nM, with a detection limit of 0.39 nM.

Keywords: FFT Coulometric Admittance Voltammetry, Theophylline, Ionic liquid, Gold nanoparticles, MWCNT

1. INTRODUCTION

Theophylline (TPL, 1,3-dimethyl xanthine) is a bronchodilator, which is extensively used in the cure of asthma and bronchospasm in adults [1]. Asthma is an inflammatory disease characterized by

bronchial hyper-responsiveness that can progress life-threatening airway obstruction [2]. Theophylline structure is shown in Scheme 1. This drug has been the cornerstone of asthma management for 80 years and it is still an important drug in the treatment of this disease, especially for patients with moderate-to-severe symptoms [3]. TPL is commonly prescribed for pediatric patients with asthma, other forms of reactive airway disease and apnea of prematurely [4].



Scheme 1. Chemical structure of Theophylline.

Up to now, several instrumental methods for measurement of TPL have been reported, for example, spectrophotometry [5-7], liquid chromatography [8-10], fluorimetry [11], solid-phase extraction [12] and electrochemical techniques [13-17]. Among these techniques, electrochemical methods offer good characteristics such as, simplicity, high sensitivity with a low-cost instrumentation and on-site monitoring. Therefore, designing of new electrochemical sensors for TPL detection has attracted a great deal of attention.

Development of nano-science and nanotechnology presents new nanomaterials for fabrication of chemically modified electrodes [18-29]. In this direction, different kinds of nanoparticles have been used in modification and construction of various sensors. The exceptional characteristics of gold nanoparticles (Au NPs) offer a appropriate environment for electron transfer between the analyte and electrode [30]. In addition, using of Au NPs incorporation with other nanomaterial, such as carbon nanomaterials, can efficiently enhancing the electron transfer reactivity of surface of the electrode [31].

In fact, the nanomaterials of carbon, such as multiwall carbon nanotubes (MWCNTs) can provide high surface area along with a good electrical conductivity for developing electrodes. Furthermore, such materials could establish a larger number of active sites to adsorb more analyte molecules, which have led to a wide use of this nanomaterial in structure of electrochemical sensors and biosensor [32- 37]. The mixture characterizations of MWCNT and Au NPs enhance the redox reaction of analyte species [38-40].

In this study, a new nanocomposite electrode was proposed for determination of TPL using FFT Coulometric Admittance Voltammetry (FFTC AV) technique in a flow injection system for the first time. The electrode was constructed by deposition of gold nanoparticles on mixture of carbon multiwall nanotube and Chitosan casted on a carbon paste electrode containing SiC NPs and ionic liquid. Ionic liquid (IL) have been used as a binder in the content of carbon paste electrode to improve

the performance, ionic conductivity, stability and biocompatibility [41,42]. This nanocomposite sensor offers an improvement in the sensitivity of the TPL determination. For characterize the sensor surface. Impedance spectroscopy (EIS) and Scanning electron microscopy (SEM) was used.

2. MATERIALS AND METHODS

2.1. Reagents

1-ethyl-3-methyl-imidazolium ethylsulphate (IL) was obtained from Aladdin-Reagent Company (China). Silicon carbide (SiC) powders with average particle size of 10-25 nm, supplied by IROC Corporation, Iran. MWCNTs (greater-or-equal, slanted 95% purity), Chitosan (CHT), HAuCl_4 and Theophylline were purchased from Sigma–Aldrich. Graphene nanosheets purchased from Sinopharm Henan Bonzer Imp. All other chemicals were obtained from Sigma–Aldrich. Buffer solution ($\text{NaH}_2\text{PO}_4/\text{Na}_2\text{HPO}_4$, 0.05 M at pH 4.5) was used as the supporting electrolyte. Double distilled water was used throughout the experiment. For the measurements a solution of 2mM of TPL was prepared and for obtaining an appropriate concentration an aliquot was diluted.

2.2. Sensor fabrication

A schematic step of the sensor preparation is shown in Fig.1. The carbon paste Si IL electrode, CILSiCE, was fabricated by hand-mixing of 4 g graphite powder, 2g SiC NPs and 2 g of IL in a mortar, and then the mixture was heated to form a homogeneous carbon paste. The paste was packed into a cavity of Teflon tube (i.d. 3.1 mm) then an electrical contact was established via a copper wire to the paste in the inner hole of the tube. A mirror-like surface was obtained by smoothing the electrode onto a weighing paper and it was then left to cool to room temperature.

To obtain functionalized MWCNT (FMWCNT), the MWCNTs were functionalized by sonochemical treatment in acidic solution [43]. Typically, the MWCNTs were mixed with 3 M HNO_3 (25 mL) and sonicated for 7 h at room temperature. The sonicated MWCNTs were repeatedly washed with methanol and Millipore water and dried in vacuum.

The stock solution of 1% CHT was prepared by dissolving 0.1 g of CHT to 10 mL of 1:1 – ethanol: H_2O solution under stirring conditions and maintaining a pH 3 through the addition of 0.1 M HCl. The undissolved material was filtered. Then, the pH value was gradually adjusted to pH 6.0 by adding 0.1 M NaOH. Finally, the obtained filtrate solution was appropriately diluted to a 0.5% CHT solution.

The CHT-MWCNT (or FMWCNT) nanocomposite was obtained by dispersing 1.2 mg of MWCNTs in 1 mL of CHT (0.5% in 1:1 – ethanol: H_2O solution) with the aid of ultrasonic stirring for 30 min. The MWCNTs-CHIT dispersion was kept at 4 °C when not in use and was stable for at least 5 months. Then, 20 μL of the CHT-MWCNT nanocomposite was cast on the surface of well-polished CILSiC electrode, and then the electrode was rinsed with doubly distilled water. For obtaining

AuNPs/MWCNT-CHT/CILSiCE, the electrochemical deposition of Au NPs was done in 0.2 M Na_2SO_4 aqueous solution of HAuCl_4 (1.0 mM) at the potential of -0.20 V for 80s.

2.3. Electrochemical detection

The equipment for flow injection was an integrated analysis which has a five way injection valve (Ultratech Labs Co., Iran) with 600 μL sample injection loop, an eight roller peristaltic pump (Ultratech Labs Co., Iran) and an electrochemical cell setup which are shown in Fig. 2A. The electrochemical cell was a conventional three-electrode system with a working electrode, a platinum wire as an auxiliary electrode and a saturated calomel electrode (SCE) as reference electrode.

A homemade potentiostat was used for the electrochemical FFTCAV measurements. It was connected to a PC equipped with an analog to digital data acquisition board (PCL-818H, Advantech Co.). The developed program software was used to generate an analog waveform and acquire current readings. A modified form of potential waveform was continuously applied to the working electrode (shown in Fig. 2B). As displayed in the figure, the measurement part of the waveform contains a multiple SW polarization cycle with amplitude of E_{sw} and frequency of f_o , were superimposed on a staircase potential which was changed by a small potential step of ΔE (10 mV). The value of E_{sw} was in the range of 5 to 100 mV.

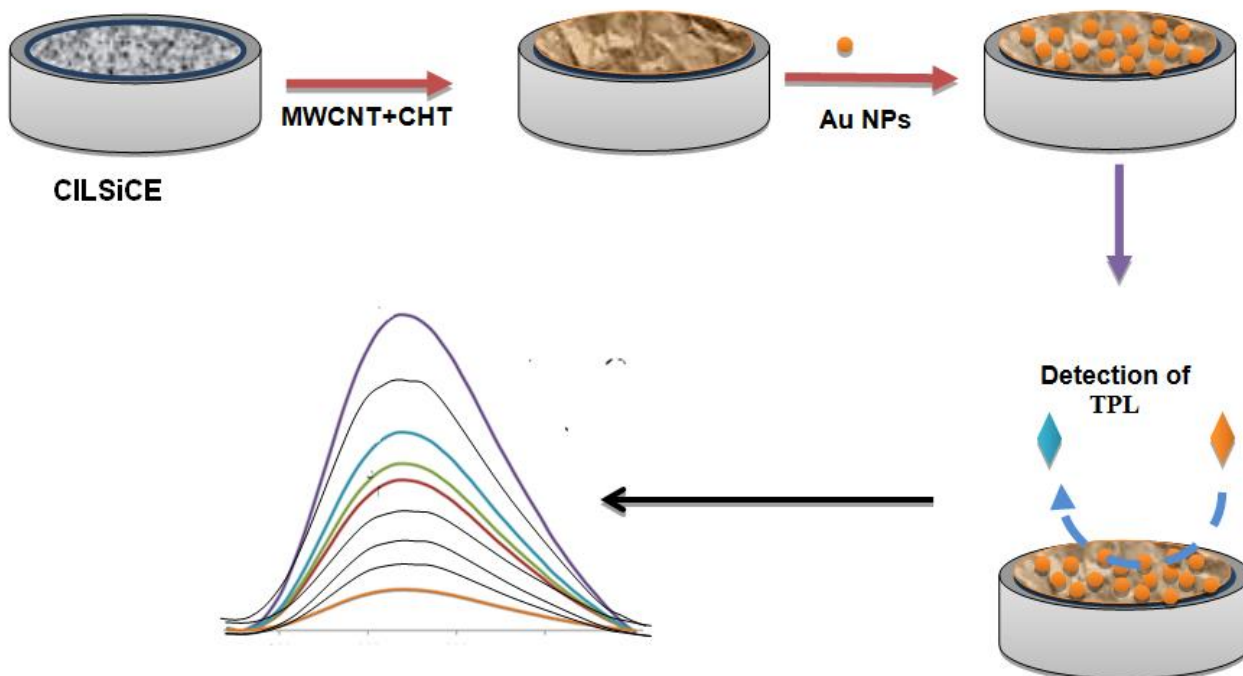


Figure 1. A schematic phases of the sensor fabrication

In the potential ramp, the currents were sampled eight times per each SW polarization cycle. This is the advantages of FFTCAV that was used signal averaging to enhance the S/N. FFTCAV technique is able to sample the current across the entire a SW period, which are used for calculating the admittance of the sensor[44-48]. In this direction, the software was able to process in real time and

plot the data. Electrochemical impedance spectroscopy (EIS) measurements were carried out in a faraday cage with AutoLab Potentiostat PGSTAT302N (Metrohm AutoLab BV, Utrecht, The Netherlands) in 3 mM $[\text{Fe}(\text{CN})_6]^{3-/4-}$ solution in 0.1M KCl.

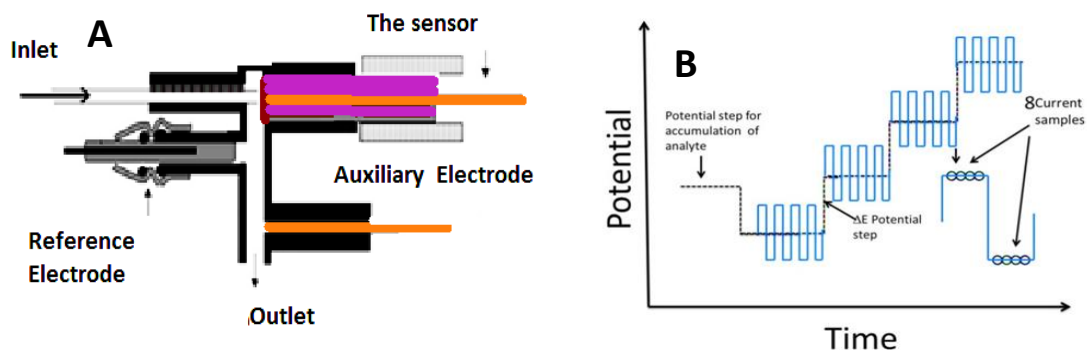


Figure 2. A) Schematic of the electrochemical cell used in flow injection analysis, B) Diagram of the potential waveform used in FFTCAV.

3. RESULTS AND DISCUSSION

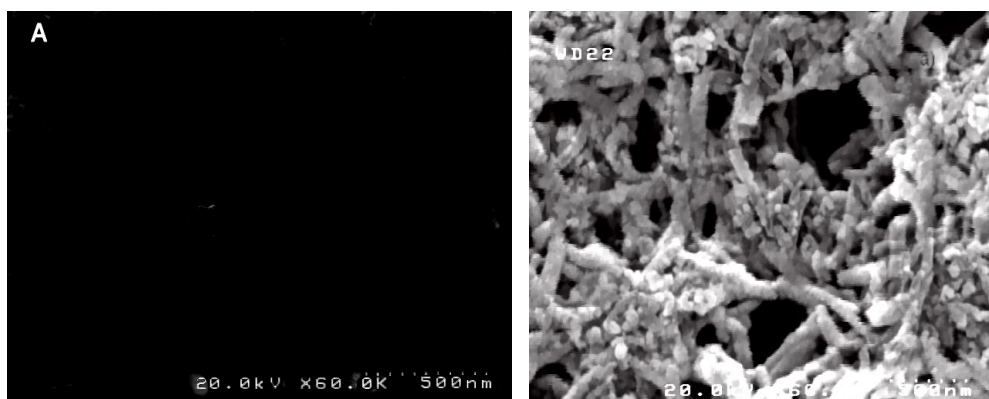


Figure 3. SEM image of A)CILSiCE, B)AuNPs/MWCNT-CHT/CILSiCE sensor.

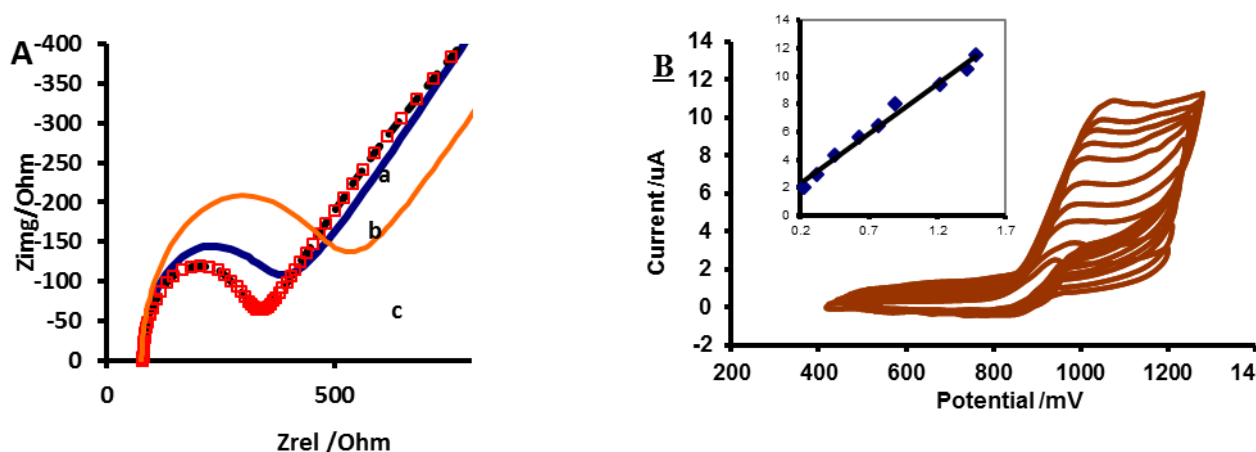


Figure 4. A) EIS plots of modified electrode in 3 mM $[\text{Fe}(\text{CN})_6]^{3-/4-}$ in 0.1 M KCl: (a) bare CILSiCE (b)MWCNT-CHT/CILSiCE, and (c) AuNPs/MWC-CHT/CILSiCE. B) Typical Cyclic voltammograms of the sensor in 3 μM TPL in 0.05 M PBS pH 4.0, at different scan rates of 0.05, 0.1, 0.2, 0.4, 0.6, 0.8, 1.5, 2.0, 2.2 V/s.

For any sensor, the analyte response is effected by its morphology. Therefore, the morphology of the surface of the electrode was examined by SEM technique. As shown in Fig. 3A and B, the SEM images of the CILSiCE and AuNPs/MWCNT-CHT/CILSiCE present the successful of modification of the electrode surface. In fact in Fig. 3B, AuNPs were made on the composite surface by electrodepositing at -200 mV from HAuCl_4 solution as described above. As shown, AuNPs were uniformly distributed on the working electrode surface.

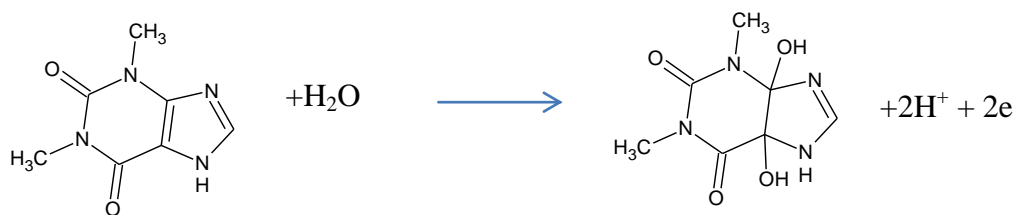
The typical crumpled structure shows along with amount of MWCNT surface can be seen in the figure. Similarly, in some parts of the SEM image for AuNPs/MWCNT-CHT/CILSiCE, a granular morphology with average grain size of about 140 nm can be observed.

The EIS curves for the unmodified CILSiCE, MWCNT-CHT/CILSiCE and AuNPs/MWCNT-CHT/CILSiCE in 0.1 M KCl solution containing 3 mM $[\text{Fe}(\text{CN})_6]^{3-/4-}$, respectively, is shown in Fig. 4A. The curves showed that R_{ct} (charge transfer resistance) of MWCNT-CHT/CILSiCE (curve b). It was lower than that was seen for the bare CILSiCE electrode (curve a) due to a higher collection of $[\text{Fe}(\text{CN})_6]^{3-/4-}$ and larger surface area. Also, for AuNPs/MWCNT-CHT/CILSiCE (curve c), the value of R_{ct} decreased, due to highly electrical conductivity of AuNPs. This can improve the electron transfer value at the electrode surface for $[\text{Fe}(\text{CN})_6]^{3-/4-}$.

3.1. Determination of TPL

Fig. 4B showed the CVs of 3 μM TPL in 0.05M PBS (pH 4.0) on AuNPs/MWCNT-CHT/CILSiCE at scan rates of $0.05, 0.1, 0.2, 0.4, 0.6, 0.8, 1.5, 2.0, 2.2$ V/s. Over the applied potential range, a lesser redox activity is observed for the unmodified CILSiC electrode. In the CV curves, there is a well-defined oxidation peak on the modified electrode about 1.1 V. A more conceivable mechanism for TPL electrode reaction is shown in Scheme 2.

In the figure, it appears the modified electrode cause a significant reduction currents. This point to catalyze effect of modifier on the electrochemical process. However, in all of the CVs, there is very low reduction current in the reversed scan which indicates the oxidation processes is close to irreversible process. Also, the inset curve in the figure 4B shows the influence of the square root of the scan rate on the peak current and the equation can be expressed in a linear equation ($I_p = 56 v^{1/2} + 0.51$; $r = 0.99$) which is of a typical diffusion controlled process.



Scheme 2. Possible electrode reaction mechanism for TPL

A three dimensional background subtracted admittance voltammogram curves, in the potential range of 200 to 1400 mV, are shown in Fig. 5, in which the time axis symbolizes the time length of the experiment. As shown in the figure, at the beginning of the experiment there is no current in the voltammograms, then a peak appears at potential of 500 mV, after addition of 2.0×10^{-7} M TPL in 0.05 M PBS. The admittance peak could be result of the electrochemical reaction of TPL at AuNPs/MWCNT-CHT/CILSiCE.

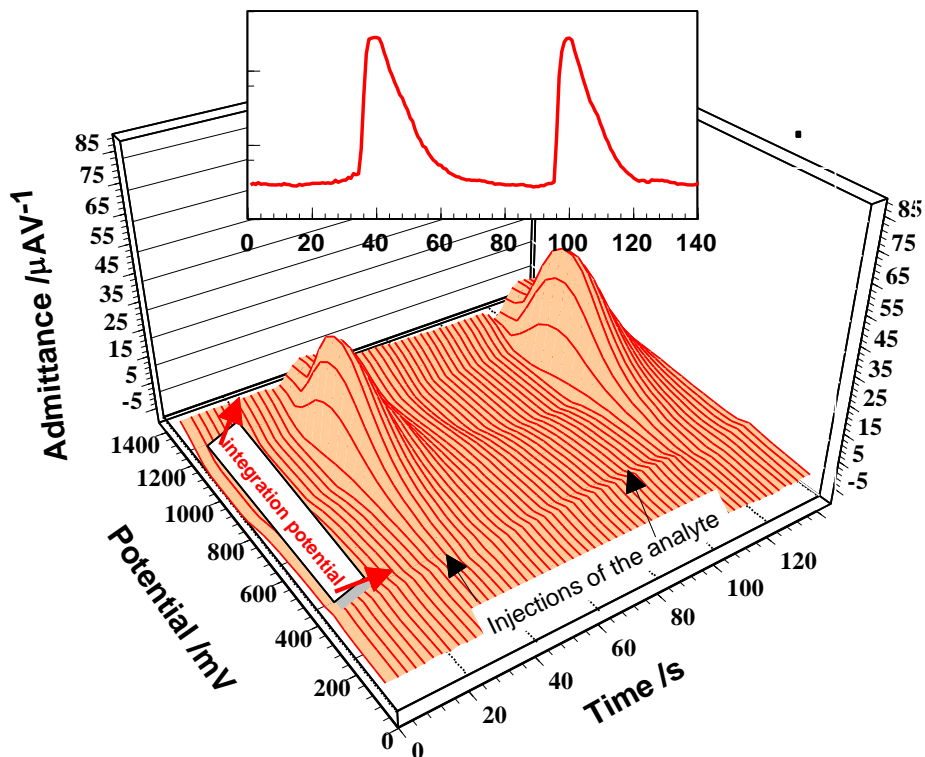


Figure 5. FFT admittance voltammograms before and after addition of 2.0×10^{-7} M TPL in buffer solution at pH 4.0, at AuNPs/MWCNT-CHT/CILSiCE; at frequency 400 Hz and amplitude 25 mV. The inset graph is the electrode response, after integration in potential from 300 to 1100 mV of the admittance.

For measurement, the analyte response was obtained by the computing of the absolute charge changes in the recorded admittances [49-55]. Consequently, response is in form of coulomb (C), which is the charge changes (ΔQ) under the voltammograms at a selected potential range, E_1 to E_2 :

$$\Delta Q_n = Q_n - Q_{ave} \quad \text{for } n > 0 \tag{1}$$

or

$$\Delta Q_n = \Delta t \left[\int_{E_1}^{E_2} A(s, E).E dE + ave \int_{E_1}^{E_2} A(s, E).E dE \right] \tag{2}$$

$$\Delta Q (s \tau) = \Delta t \left[\sum_{E=E_1}^{E=E_2} A(s, E).E - \sum_{E=E}^{E=E_2} A(s_r, E).E \right] \tag{3}$$

where Q is the calculated charge which is integration of admittance voltammetric curve between 300 and 1100 mV and Q_0 represents Q in the absence of the adsorbent, s is the sweep number, τ is the time period between subsequent sweeps, Δt is the time difference between two subsequent points on the FFTCAV curves, $A(s, E)$ is the admittance of the electrode during the s^{th} scan, and $A(s_r, E)$ is the reference admittance. Here, the calculated reference admittance was obtained by averaging a few FFTCAV curves (3-5) recorded at the beginning of the run before injection of the analyte. The optimization of important parameters such as the FFTCAV amplitude and frequency and flow rate, the electrochemical response or S/N was enhanced.

3.2. Optimization of FFTCAV frequency and amplitude

The SW frequency performances alike to potential scan rate in cyclic voltammetry technique, the value of the background noise and response shape rely on condition of the excitation potential waveform. Therefore, the value SW frequency and amplitude are essential elements in sensitivity of the coulometric response of AuNPs/MWCNT-CHT/CILSiCE.

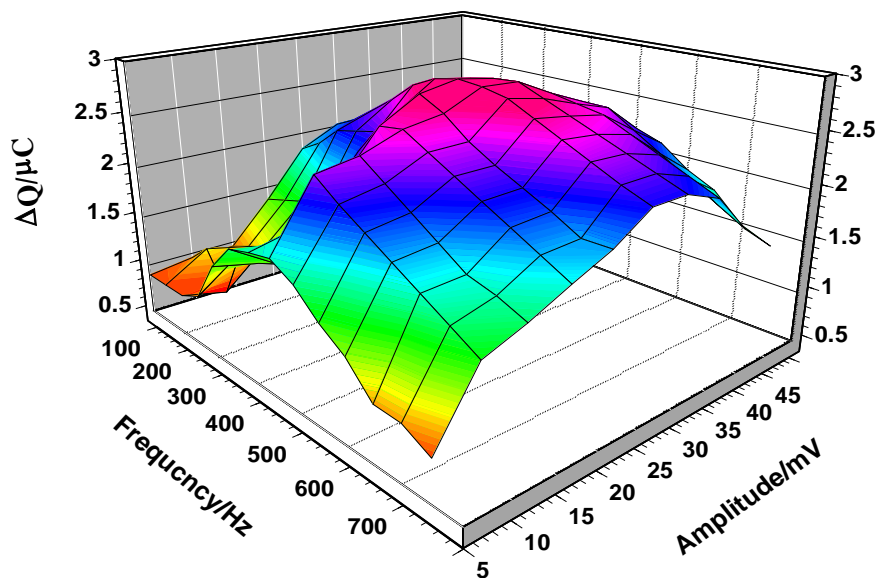


Figure 6. The dependency of response of AuNPs/MWCNT-CHT/CILSiCE in 2.0×10^{-7} M TPL in buffer solution at pH 4.0 to the frequency and amplitude, where the potential range was 300 to 1100 mV.

To obtain the optimum SW waveform condition for maximum ΔQ , the SW frequency of range 100-700 Hz and amplitude of 5 to 50 mV were studied. In Fig. 6 the importance of frequency and amplitude is demonstrated for solution of 2.0×10^{-7} M of TPL. As shown in the graph, an enhancement in the SW frequency or amplitude causes the response value of the electrode increases. Consequently, up to 400 Hz and amplitude up to 25 mV, the value of ΔQ increases and after that a decreases. In fact,

the SW frequency increasing causes the sensitivity increased, may due to gaining a higher charging/faradic current ratio. Here, the solution resistance, electrode diameter and stray capacitance of the electrochemical system will limit the sensitivity gains may obtained by the enhancing the SW frequency. Also, it could be proposed that at the higher values of frequency and amplitude, due to small time for the electrochemical reaction on the surface, the response becomes smaller. In FFTCAV technique, application of SW frequencies lower than 400 Hz causes a longer potential scan times which results lower voltammetric scans (as well as the admittance values in the response peak for each injected sample).

3.3. The nanocomposite condition

The variation of the analyte response with the amount of MWCNT and Au NPs in the content of the modifier composition is presented Fig. 7. Where, for calculating the response of the electrode at the frequency of 400 Hz and 25 mV amplitude, the potential range for ingratiation was 300 to 1100 mV. Also, the injected sample was 2.0×10^{-7} M TPL in the buffer solution at pH 4.0. In these experiments, the deposition times for forming Au NPs was in range of 20 to 200 s. Also, various amounts of MWCNT (0.1 to 2.5 mg) in suspension solution were casted on the electrode surface.

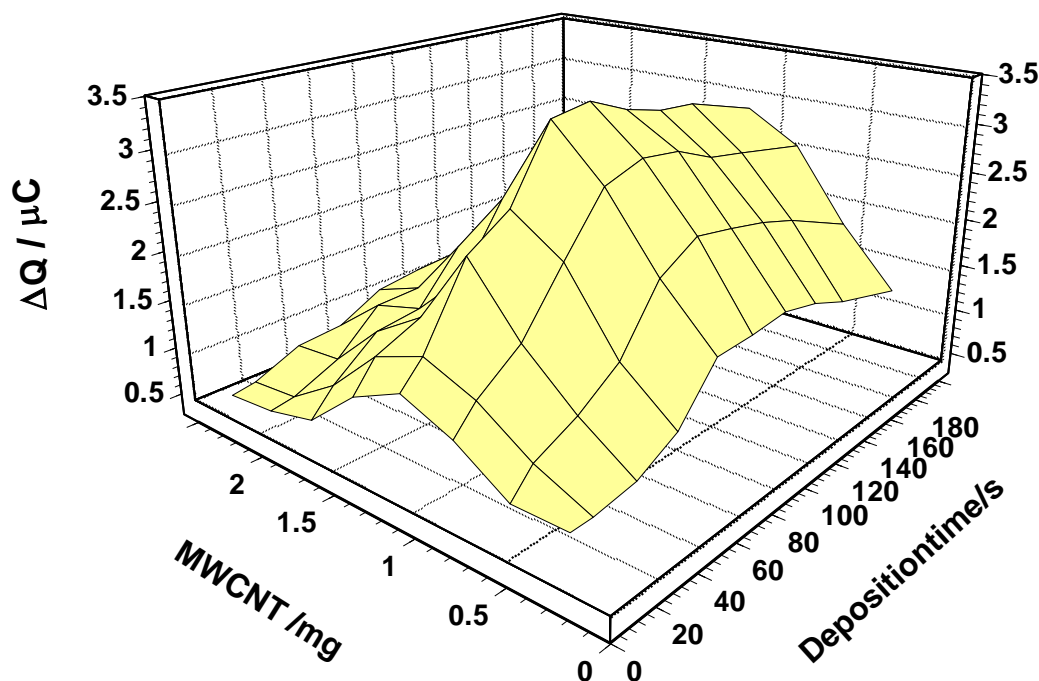


Figure 7. The change of AuNPs/MWCNT-CHT/CILSiCE response for 2.0×10^{-7} M solution of TPL at pH 4.0, by the change of deposition time for Au NPs and amount of MWCNT. The voltammograms were recorded at frequency 400 Hz and amplitude 25 mV, in the potential

range of -200 to 1400 mV. The response was calculated in potential range for the admittance was 300 to 1100 mV

The curve specifies the value of the response rises with the increasing of MWCNT up to 1.2 mg and then diminutions. Moreover, as shown in figure, for Au NPs the value of ΔQ increases with increasing the deposition time for Au NPs on the sensor composition up to 80 s and then decreases with increasing of this time. Such data could be results of the dispersion of the AuNPs size, and it becomes larger with the increasing electrodeposition time. However, the value of ΔQ stayed almost unchanged at the greater volume of Au NPs solution, which could be result of constant surface area of the electrode.

3.4. Analytical performance

The electrode process of TPL on the electrode surface can enhance the response of sensor. The calibration curve for TPL was obtained by applying in optimal experimental conditions for FFTCAV method. Fig. 8 displays the value of ΔQ for AuNPs/ MWCNT-CHT/CILSiCE displays a dynamic correlation with the concentration in the range from 0.2 to 500.0 nM of TPL in buffer solution at pH 4.0 .

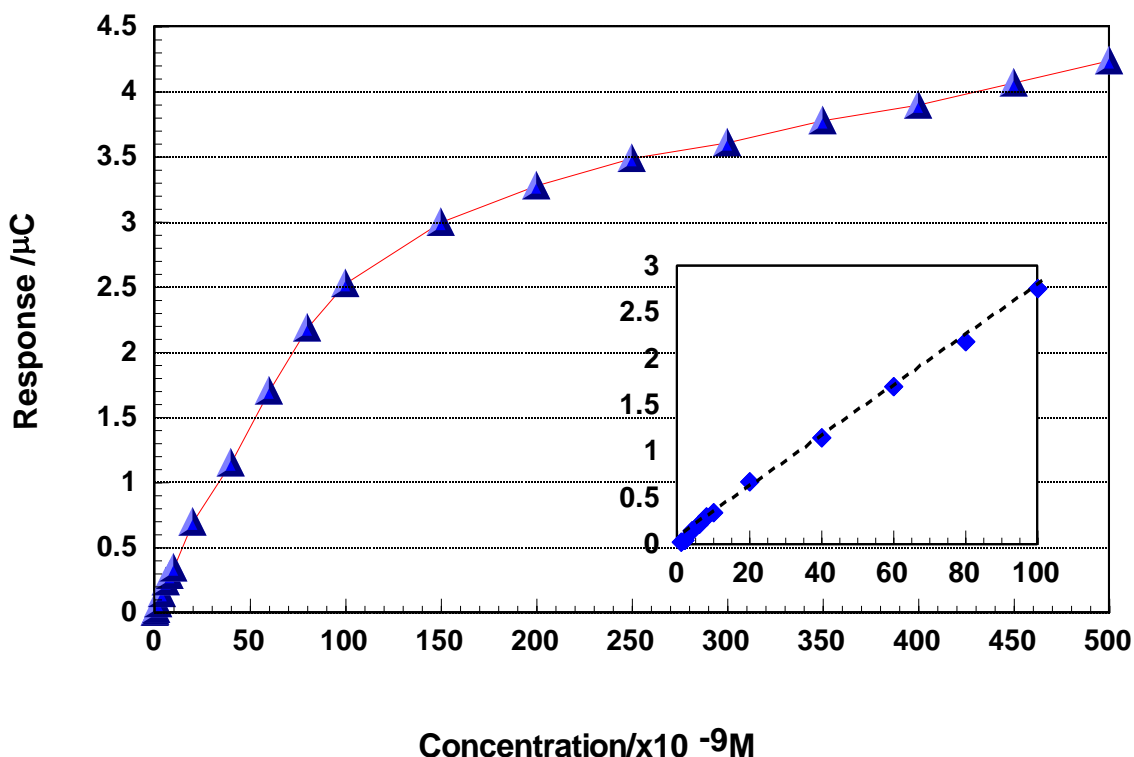


Figure 8. Response of the AuNPs/MWCNT-CHT/CILSiCE in TPL 0.2 to 500 nM in buffer solution at pH 4.0. The voltammograms were recorded in the potential range of 300 to 1100 mV at frequency of 400 Hz and amplitude of 25 mV. The linear range of calibration curve is in the inset graph.

Where the voltammograms were recorded in the potential range of 300 to 1100 mV at the frequency of 400 Hz and amplitude of 25 mV. Each data point in the calibration curve represents the average of 3 consecutive sensor responses to the injection of the standard solution of TPL. In the figure inset, the linear part of the calibration curve is shown. Obtained regression equation with a correlation coefficient of $R^2 = 0.993$, for this part of the calibration curve, was $\Delta Q (\mu\text{C}) = 0.132x + 0.035$ (nM). The predictable detection limit based on signal to noise ratio (S/N=3), was found 3.9×10^{-10} M. Also, the proposed sensor was used for measurement of TPL in spiked real samples. Correspondingly, the response time of the sensor was about 6s.

The results are shown in Table 1. The experimental data specified a reliable recovery for the sensor. The results indicated that the proposed electrode could be applied effectively for the determination of TPL in real samples using this method.

Table 1. Recovery% of TPL from certified reference

Added (nM)	Found (nM)	Recovery (%)
8.0	7.3	97.0
10.0	9.65	96.5
12.5	12.43	99.0
25.0	24.7	99.3
50.0	47.70	98.7
75.0	74.4	98.4
100.0	94.60	94.2

AuNPs/MWCNT-CHT/CILSiCE was tested in 90 days. It showed a long-term storage stability, and the sensitivity only decline to 97.8%. Then, it slowly decreases might be result of the losing of some the nanomaterial in the solution. In addition, the performance of the sensor was compared with some of the best previously reported ones (Table 2) and it was confirmed that the presented electrochemical based TPL sensor with FFTCAV technique confirmed an excellent sensitivity [16, 56-64].

Table 2. The comparison of the proposed electrochemical sensor with some of the previous reported ones for TPL detection.

Detection method	DL	Materials	Ref.
Differential pulse voltammetry	0.4 μM	CdSe microparticles modified glassy carbon electrode	[16]
Differential pulse voltammetry	1.85×10^{-7} M	Carbon Paste Electrode	[56]
Differential pulse voltammetry	1.6×10^{-8} M	aligned carbon nanotubes (ACNTs) thin film modified electrode	[57]
Differential pulse voltammetry	1 μM	Dopamine Self-Polymerization	[58]

Differential pulse voltammetry	1 μ M	sol-gel immobilized molecularly imprinted polymer r	[59]
Differential pulse anodic stripping voltammetry	1.4×10^{-9} M	glassy carbon electrode modified with imprinted sol-gel film immobilized on carbon nanoparticle layer	[60]
Differential pulse voltammetry	3 nM	WS ₂ nano-flowers/silver nanoparticle composite modified glassy carbon electrode	[61]
Amperometry	0.32 μ M	Molecularly imprinted poly(4-amino-5-hydroxy-2,7-naphthalenedisulfonic acid) modified glassy carbon electrode	[62]
Cyclic voltammetry	0.1 μ M	Manganese dioxide nanosheet-decorated ionic liquid-functionalized graphene	[63]
Differential pulse voltammetry	1.2 nM	SiO ₂ @TiO ₂ -based imprinted polymer composite	[64]
FFTCV	3.9×10^{-10} M	AuNPs/MWCNT-CHT/CILSiCE	This work

4. CONCLUSIONS

In this work, an ultra-sensitive measurement electrochemical system was successfully used for TPL determination. The sensor fabricated by modification the CILSiCE surface with AuNPs/MWCNT-CHT. The electrochemical FFTCAV technique (which developed in our lab) was employed to improve the sensitivity of the sensor. The sensor exhibited good analytical characteristics, such as higher affinity of TPL towards AuNPs/MWCNT-CHT/CILSiCE with a good repeatability and reproducibility. The new composite modifier has shown a good example for the interaction of TPL and NPs and nanostructures. Finding a reproducible measurement for sensor with response time less than 6 s and detection limit of 0.39 nM, can be consider an important achievement for this drug, which can open a new application for FFTCAV technique, as sensitive tool, for trace analysis of drugs in real sample.

ACKNOWLEDGEMENT

The authors are grateful to the Research Council of University of Tehran for the financial support of this work.

References

1. P.J. Barnes, American Journal of Respiratory and Critical Care Medicine, 188 (2013) 901.
2. G. W. Canonica, *CHEST Journal*, 130 (1_suppl) (2006) 21S.
3. N. Scichilone, et al., *European journal of internal medicine*, 25 (2014) 336.

4. E.A. Lancet, J. T. Holbrook, R. A. Wise, and N. A. Hanania, *Clinical Investigation*, 4 (2014) 495.
5. S.K. Hassaninejad-Darzi, A. Samadi-Maybodi, and S.M. Nikou, *Iranian Journal of Pharmaceutical Research*, 15 (2016) 379.
6. D.G. Zanzarukiya, and J.S. Shah, *JPSBR*, 4 (2014) 139.
7. L. Jing, Q. Zhang, Y. Wang, X. Liu, and T. Wei, *Anal. Methods*, 8 (2016) 2349.
8. Y. Lin, Y. Zhang, Y. Zhang, X. Chen, and D. Zhong, *Curr. Pharm. Anal.*, 12 (2016) 296.
9. M. Charehsaz, *Iranian journal of pharmaceutical research: IJPR*, 13 (2014) 431.
10. Xi-xian, C., L. Jian-xin, and L. Dong, *Chinese Journal of Hospital Pharmacy*, (1994) 9.
11. C.M. Rico, et al. *Analyst*, 1995. 120 (1995) 2589.
12. W.M. Mullett, and E.P. Lai, *Anal. Chem.*, 70 (1998) 3636.
13. S. Mansouri-Majd, et al., *Electrochim. Acta*, 108 (2013) 707.
14. S. Tajik, M.A. Taher, and H. Beitollahi, *Sens. Actuators B*, 197 (2014) 228.
15. G. Yang, F. Zhao, and B. Zeng, *Talanta*, 127 (2014) 116.
16. H. Yin, X. Meng, H. Su, M. Xu, and S. Ai, *Food Chemistry*, 134 (2012) 1225.
17. J.M. Zen, T.Y. Yu, and Y. Shih, *Talanta*, 50 (1999) 635.
18. A. Chen, and S. Chatterjee, *Chem. Soc. Rev.*, 42 (2013) 5425.
19. J. T. Mehrabad, M. Aghazadeh, M. R. Ganjali, P. Norouzi, *Mater. Lett.*, 184 (2016) 223.
20. I. Karimzadeh, M. Aghazadeh, T. Dourudi, M. R. Ganjali, and P. H. Kolivand *Curr. Nanoscience*, 13 (2017) 167.
21. M. Aghazadeh, M. G. Maragheh, M. R. Ganjali, and P. Norouzi, *Inorganic and Nano-Metal Chemistry* 27 (2017) 1085.
22. S. Tajik, M.A. Taher, and H. Beitollahi, *Sens. Actuators B*, 197 (2014) 228.
23. M. Aghazadeh, M. R. Ganjali, *J Materials Science Materials in Electronics* 28 (2017) 8144.
24. I Karimzadeh, M Aghazadeh, MR Ganjali, P Norouzi, and T Doroudi, *Mater Lett*, 189 (2017) 290.
25. M.R. Akhgar, H. Beitollahi, M. Salari, H. Karimi-Maleh, and H. Zamani, *Anal. Methods*, 4 (2012) 259.
26. M. Aghazadeh, I. Karimzadeh, M. R. Ganjali, M. M. Morad, *Mater. Lett.* 196 (2017) 392.
27. M. Aghazadeh, M. Asadi, M. R. Ganjali, P. Norouzi, B. Sabour, and M. Emamalizadeh, *Thin Solid Films* 634 (2017) 24.
28. H. Karimi-Maleh, M.R. Ganjali, P. Norouzi, A. Bananezhad, *Materials Science and Engineering C* 73 (2017) 472.
29. J. Shabani Shayeh, A. Ehsani, M. R. Ganjali, P. Norouzi, B. Jaleh, *Applied Surface Science*, 353 (2015) 594.
30. K. Saha, S. S. Agasti, C. Kim, X. Li, and V. M. Rotello, Gold nanoparticles in chemical and biological sensing. *Chem. Rev.*, 2012. 112(5): p. 2739-2779.
31. M.L. Yola, and N. Atar, *Electrochim. Acta*, 119 (2014) 24.
32. Baptista, F.R., et al., Recent developments in carbon nanomaterial sensors. *Chem. Soc. Rev.*, 44 (2015) 4433.
33. M. Holzinger, A. Le Goff, and S. Cosnier, *Frontiers in Chemistry*, (2014) 2, doi.org/10.3389/fchem.2014.00063.
34. H. Beitollahi, J.B. Raoof, and R. Hosseinzadeh, *Anal. Sci.*, 27 (2011) 991.
35. M.M. Foroughi, H. Beitollahi, S. Tajik, M. Hamzavi, and H. Parvan, *Int. J. Electrochem. Sci.*, 9 (2014) 2955.
36. M. Mazloun-Ardakani, B. Ganjipour, H. Beitollahi, M.K. Amini, F. Mirkhalaf, H. Naeimi, and M. Nejati-Barzoki, *Electrochim. Acta*, 56 (2011) 9113.
37. H. Beitollahi, J.B. Raoof, H. Karimi-Maleh, R. Hosseinzadeh, *Journal of Solid State Electrochemistry*, 16 (2012) 1701.
38. E. Dilonardo, M. Penza, M. Alvisi, C. Di Franco, R. Rossi, F. Palmisano, L. Torsi, and N. Cioffi, *Sensors and Actuators B*, 223 (2016) 417.
39. J. Dong, et al., *Sensors and Actuators B*, 186 (2013) 774.

40. J. Dong, et al., *Food Chemistry*, 141 (2013) 1980.
41. M. Elyasi, M.A. Khalilzadeh, and H. Karimi-Maleh, *Food Chemistry*, 141 (2013) 4311.
42. M. Najafi, M.A. Khalilzadeh, and H. Karimi-Maleh, *Food Chemistry*, 158 (2014) 125.
43. F. Avilés, et al., *Carbon*, 47 (2009) 2970.
44. P. Norouzi, H. Haji-Hashemi, B. Larijani, M. Aghazadeh, E. Pourbasheer and M. R. Ganjali, *Curr. Anal. Chem.*, 13 (2017) 70.
45. P. Norouzi, V. K. Gupta, B. Larijani, S. Rasoolipour, F. Faridbod and M. R. Ganjali, *Talanta*, 131, (2015) 577.
46. P. Norouzi, B. Larijani, M. R. Ganjali and F. Faridbod, *Int. J. Electrochem. Sci.*, 9 (2014) 3130.
47. P. Norouzi, B. Larijani, F. Faridbod and M. R. Ganjali, *Int. J. Electrochem. Sci*, 8 (2013) 6118.
48. S. Jafari, F. Faridbod, P. Norouzi, A. S. Dezfuli, D. Ajloo, F. Mohammadipanah and M. R. Ganjali, *Anal. Chim. Acta*, 895 (2015) 80.
49. P. Norouzi, M. R. Ganjali, and P. Matloobi, *Electrochem. Commun.*, 7 (2005) 333.
50. P. Daneshgar, P. Norouzi, and M.R. Ganjali, *Sensors and Actuators B: Chemical*, 136 (2009) 66.
51. P. Norouzi, M. R. Ganjali, and L. Hajiaghababaei, *Anal. Lett.*, 39 (2006) 1941.
52. P. Norouzi, M. R. Ganjali, A. Sepehri, and M. Ghorbani, *Sens. Actuators B*, 110 (2005) 239.
53. P. Daneshgar, P. Norouzi, M. R. Ganjali, A. Ordikhani-Seyedlar and H. Eshraghi, *Colloid Surface B*, 68 (2009) 27.
54. P. Daneshgar, P. Norouzi, M. R. Ganjali and H. A. Zamani, *Talanta*, 77 (2009) 1075.
55. V. K. Gupta, P. Norouzi, H. Ganjali, F. Faridbod and M. R. Ganjali, *Electrochim. Acta*, 100 (2013) 29.
56. R.N. Hegde, R.R. Hosamani, and S.T. Nandibewoor, *Anal. Lett.*, 42 (2009) 2665.
57. W. Sun, and J. Hu, *J. Anal. Chem.*, 68 (2013) 694.
58. L. Li, L. L. Yang, Y. Teng, M. Zhong, X. J. Lu, and X. W. Kan, *J. Electrochem. Soc.*, 161 (2014) B312.
59. F. Bates and M. del Valle, *Microchim. Acta*, 182 (2015) 933.
60. S. Güney and F. Ç. Cebeci, *Sensor Actuat B-Chem*, 208 (2015) 307.
61. H. B. Wang, H. D. Zhang, Y. H. Zhang, H. Chen, L. L. Xu, K. J. Huang and Y. M. Liu, *J. Electrochem. Soc.*, 162 (2015), B173.
62. K. K. Aswini, A. M. Vinu Mohan and V. M. Biju, *Mat. Sci. Eng. C*, 65 (2016) 116.
63. X. Zhuang, D. Chen, Sh. Wang, H. Liu and L. Chen, *Sensor Actuat B-Chem*, 251 (2017) 185.
64. T. Gan, A. Zhao, Zh. Wang, P. Liu, J. Sun and Y. Liu, *J. Solid State Electr.* 21 (2017) 1 (Article in Press) doi:10.1007/s10008-017-3713-1.